

Considerations on free-surface detachment and bed entrainment of fluvial plastics

Matthias Kramer¹

¹UNSW Canberra, School of Engineering and Technology, Canberra, ACT 2610, Australia

Key Points:

- Novel formulation for surface detachment velocity of floating plastics
- Interrelation between plastic and sediment Shields parameters

Corresponding author: Matthias Kramer, m.kramer@unsw.edu.au

Abstract

Over the last decade, fluvial plastics have been identified as major threat to aquatic environments and human health. In order to develop adequate mitigation strategies for plastic pollution, a fundamental process understanding of riverine plastic transport is of significant importance. In this context, the implementation of research findings into numerical simulation environments is anticipated to enhance modelling capabilities and to support a rigorous decision making. Recent experimental research has focused on the incipient motion of plastic particles, as well as on the effects of surface tension on plastic concentration profiles. While these investigations have advanced the state-of-the-art knowledge, current literature still displays a lack of basic insights into layer-specific plastic transport physics. In this study, first principles are applied to advance knowledge on free-surface detachment and bed entrainment of fluvial plastics. A novel relationship for the critical surface detachment velocity is derived, followed by the development of a framework that allows to relate plastic Shields parameters to those of natural sediments. Overall, it is anticipated that these developments will trigger new research within the plastics community, and it is hoped that present findings will be implemented into Lagrangian particle tracking software.

1 Introduction

In recent years, the mechanics of fluvial plastic transport have been subject to more detailed investigations, and it was shown that different layers of plastic transport can be distinguished, including bed layer, suspended layer, and surface layer. This distinction is important, as these layers are governed by different flow physics. For example, plastic particles in the bed layer are interacting with sediment particles (Lofty et al., 2023), suspended plastics are subject to water drag and lift, while surfaced plastics are additionally influenced by air drag and surface tension (Chubarenko et al., 2016; Valero et al., 2022).

Of the three mentioned layers and associated transport modes, suspended load transport and bed load transport constitute transport processes that have been studied extensively in sediment research, and as such, sediment research can provide valuable insights for plastic research (Waldschläger et al., 2022). One prominent example of this knowledge transfer is the adaptation of the well-known Rouse equation to positively buoyant plastics, as first discussed in Cowger et al. (2021). However, it is noted that there are important differences between natural sediments and plastics in suspended load transport, which are primarily caused by varying shapes and materials. Van Melkebeke et al. (2020) reviewed drag coefficients of plastics in suspension, concluding that the approaches of Bagheri and Bonadonna (2016) and Dioguardi et al. (2018) are currently the most accurate to predict shape-dependent drag coefficients and terminal velocities of common plastics, such as disks, ellipsoids, cylinders, fibres, etc. Further, several effects on suspended particle drag and lift, including effects of turbulence, secondary motion, and hindered settling, warrant additional research.

In bed load transport, the onset of motion of plastics is of fundamental importance. This phenomenon was first investigated by Waldschläger and Schüttrumpf (2019b) for plastics on different sediment bed configurations, who related the critical plastic Shields parameter ($\theta_{cr,p}$) to the critical sediment Shields parameter ($\theta_{cr,s}$) as follows

$$\frac{\theta_{cr,p}}{\theta_{cr,s}} = c_1 \underbrace{\left(\frac{D_p}{d_{50}}\right)^{c_2}}_{\text{hiding-exposure function}}, \quad (1)$$

where D_p is the representative plastic diameter, d_{50} is the median grain size of the sediment bed, and the two empirical parameters were determined as $c_1 = 0.5588$ and $c_2 = -0.503$, the latter controlling the strength of the hiding-exposure effect. Goral et al. (2023)

interpreted the parameter c_1 as the ratio of static friction coefficients between plastic and sediment, and additionally modified the exponent of the so-called hiding-exposure function, originally introduced for sediments by [Wilcock \(1988\)](#). While Eq. (1), as well as modifications thereof, are useful for a first assessment of the incipient motion of plastic particles on sediment beds, their simplicity somewhat disguises the complexity of underlying physical processes, which is because different effects are lumped into the hiding-exposure function. In this context, it is evident that future in-depth studies of plastic re-suspension are required. According to [Rohais et al. \(2024\)](#), these studies should encompass a wider range of (micro-) plastic parameters and explore different definitions of the onset of motion, similar to those presented in [Yu et al. \(2022, 2023\)](#), aiming to derive general expressions for plastic re-suspension behaviour. Revising the literature on plastic re-suspension to date, it becomes clear that a better understanding of underlying physical processes is required, and that the applicability of sediment re-suspension models needs to be critically assessed.

Considerably less research efforts have been devoted to particle transport processes of the free-surface layer. [Chubarenko et al. \(2016\)](#) were the first to consider air drag acting on floating plastics, further deriving an expression for the relative submergence of surfaced spheres. However, [Chubarenko et al. \(2016\)](#) did not consider surface tension forces in their analysis, implying that some of their presented equations must be revised. [Valero et al. \(2022\)](#) established the key importance of surface tension forces in surface load transport, demonstrating that surface tension effects on the concentration profile can be as intense as buoyancy, and that surface tension bias can lead to a drastic underestimation of total transported plastic. Despite these advances, the common understanding of the fundamental mechanics of plastic surface load transport remains limited, and further insights are required to improve theoretical and numerical modelling capabilities.

This study aims to establish some important underpinning foundations of particle transport mechanics in the bed and the free-surface layer, comprising free-surface detachment (§ 2) and bed entrainment (§ 3) of fluvial plastics. In § 2, linear momentum conservation is applied to a floating plastic particle, enabling the derivation of a novel formulation for the particle floating velocity (§ 2.1) and the critical detachment velocity (§ 2.2). These derivations are followed by a preliminary assessment, demonstrating that the free-surface acts as sink for microplastics, regardless of their density. In § 3.1, the focus is set on the incipient motion of plastic particles, and a general formulation for the plastic Shields parameter is presented. As there is only limited experimental data available from literature, a framework that relates the plastic Shields parameter to that of natural sediment (§ 3.2) is introduced, leading to the appearance of a shape factor ratio in our expanded equations. Subsequently, this framework is applied to the literature data sets of [Waldschläger and Schüttrumpf \(2019b\)](#) and [Goral et al. \(2023\)](#) in § 3.3, and it is demonstrated mathematically that irregular shapes can lead to a reduced or increased mobility of plastics when compared to natural sediment.

2 Free-surface detachment

2.1 Floating velocity

In the following, an expression for the velocity of a floating plastic particle at the free surface is derived. Let us consider a plastic particle with sphere-volume equivalent diameter $D_p = \sqrt[3]{6\mathcal{V}_p/\pi}$, volume \mathcal{V}_p , and density ρ_p , which is floating at the free-surface of an open-channel (Fig. 1a). The particle moves with the velocity u_p and is subject to water drag $F_{D,w}$, air drag $F_{D,a}$, buoyancy F_B , surface tension F_σ , weight force F_W , and hydrodynamic lift F_L .

Implying that the acceleration of the floating particle is negligible, the acting forces are evaluated in streamwise direction, as shown in Fig. 1a, further assuming no exter-

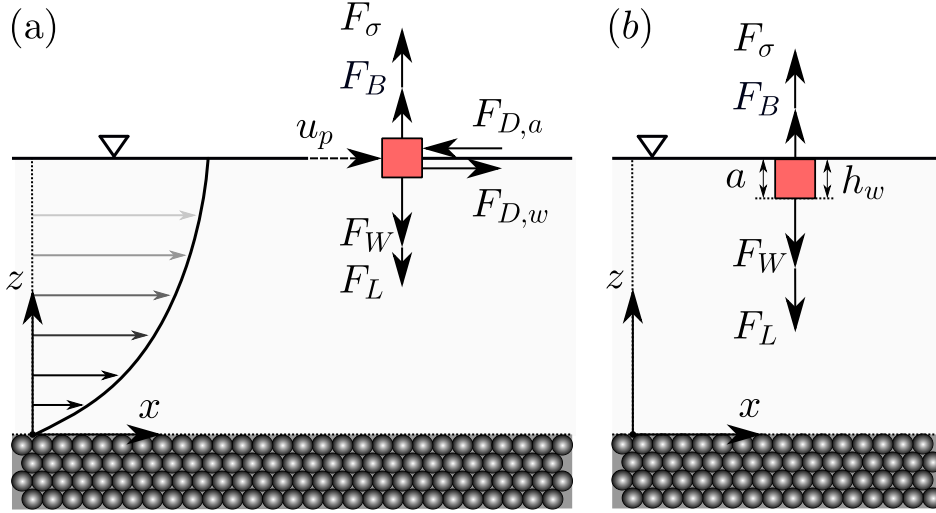


Figure 1. Floating plastic in an open-channel flow; x = streamwise coordinate, z = vertical coordinate: (a) forces acting on a floating plastic; (b) detachment condition for a cubical particle with side length a and submerged depth h_w

nal wind forcing, i.e., $u_a = u_p$, with u_a being the air velocity, yielding

$$\underbrace{\frac{1}{2} \rho_w C_D A_{\text{proj},w} |u_{\text{fs}} - u_p| (u_{\text{fs}} - u_p)}_{F_{D,w}} = \underbrace{\frac{1}{2} \rho_a C_D A_{\text{proj},a} u_p^2}_{F_{D,a}}, \quad (2)$$

where ρ_w is the water density, C_D is the drag coefficient, $A_{\text{proj},w}$ is the submerged projected surface area of the plastic particle, u_{fs} is the free-surface velocity, i.e., $u_{\text{fs}} = u(z = H)$, with u being the streamwise velocity, H the water depth, and z the vertical coordinate. Further, $A_{\text{proj},a}$ is the projected surface area of the plastic particle above the water surface, and ρ_a is the density of air. In a first approximation, C_D is assumed to be identical for the near-surface water layer and the air superlayer. Simplification leads to

$$\frac{(u_{\text{fs}} - u_p)^2}{u_p^2} = \frac{\rho_a A_{\text{proj},a}}{\rho_w A_{\text{proj},w}}, \quad (3)$$

yielding an expression for the particle velocity without wind forcing

$$u_p = \frac{u_{\text{fs}}}{\left(1 + \sqrt{\frac{\rho_a A_{\text{proj},a}}{\rho_w A_{\text{proj},w}}}\right)}. \quad (4)$$

Next, the forces acting on the plastic particle in vertical direction are considered. As discussed by Valero et al. (2022) and shown in Fig. 1, surface tension forces appear at the interfacial air-water-plastic contact line of a floating plastic particle. At this contact line, the interface bends with a certain angle, leading to a vertical component of the surface tension force. Following White (2016), the surface tension force is expressed as

$$F_\sigma = \int_{L_\sigma} \sigma \sin(\Omega) dL_\sigma \approx L_\sigma \sigma \sin(\Omega), \quad (5)$$

where σ is the surface tension, L_σ is the interfacial contact length, Ω the contact angle, and $\sin(\Omega)$ accounts for the vertical projection of the surface tension force. Further, the

floating particle is exposed to viscous surface stresses and pressures, exerted by the water phase. In the absence of detailed knowledge of the distribution of the corresponding forces across the particle's surface, these are combined into a turbulent lift force F_L , and it is anticipated that particle detachment is driven by vertical turbulent velocity fluctuations

$$F_L = \frac{1}{2} \rho_w C_{L,t} A_{\text{proj},L} v'_{\text{rms}}{}^2, \quad (6)$$

where $C_{L,t}$ is a turbulent lift coefficient, $A_{\text{proj},L}$ is the projected area for lift, and v'_{rms} is the root-mean-square of vertical velocity fluctuations. It is noted that Eq. (6) is similar to a recent formulation by [Valero et al. \(2022\)](#). Applying linear momentum conservation to the surfaced plastic in vertical direction, as per Fig. 1a, gives

$$\underbrace{\rho_w g \mathcal{V}_{p,w}}_{F_B} + \underbrace{L_\sigma \sigma \sin(\Omega)}_{F_\sigma} = \underbrace{\rho_p g \mathcal{V}_p}_{F_W} + \underbrace{\frac{1}{2} \rho_w C_{L,t} A_{\text{proj},L} v'_{\text{rms}}{}^2}_{F_L}, \quad (7)$$

where $\mathcal{V}_{p,w}$ and \mathcal{V}_p are the submerged particle volume and the total particle volume, respectively, and g is the gravitational acceleration. Subsequently, v'_{rms} is characterised using a semi-empirical relationship for open-channel flows from [Nezu and Nakagawa \(1993\)](#)

$$\frac{v'_{\text{rms}}}{u_*} = 1.27 \exp\left(-\frac{z}{H}\right), \quad (8)$$

where u_* is the shear velocity. Next, a combination of the definition of the free-surface velocity with the classical log-law for rough surfaces ([Dey et al., 2019](#)) gives

$$\frac{u_{\text{fs}}}{u_*} = \frac{1}{\kappa} \ln\left(\frac{H}{z_0}\right), \quad (9)$$

where z_0 is the hydraulic roughness. Combining Eq. (9) with Eqns. (8) and (4) leads to

$$v'_{\text{rms}}(H) = \frac{0.467 u_{\text{fs}} \kappa}{\ln\left(\frac{H}{z_0}\right)} = \frac{0.467 u_p \kappa}{\ln\left(\frac{H}{z_0}\right)} \left(1 + \sqrt{\frac{\rho_a A_{\text{proj},a}}{\rho_w A_{\text{proj},w}}}\right). \quad (10)$$

Rearrangement and combination of Eq. (7) with Eq. (10) yields another expression for the velocity of the floating plastic

$$u_p = \frac{\ln\left(\frac{H}{z_0}\right)}{0.467 \kappa} \frac{\sqrt{\frac{\rho_w g \mathcal{V}_{p,w} - \rho_p g \mathcal{V}_p + L_\sigma \sigma \sin(\Omega)}{\frac{1}{2} \rho_w C_{L,t} A_{\text{proj},L}}}}{1 + \sqrt{\frac{\rho_a A_{\text{proj},a}}{\rho_w A_{\text{proj},w}}}}. \quad (11)$$

A dimensionless form can be obtained by dividing Eq. (11) with $\sqrt{\left(\frac{|\rho_w - \rho_p|}{\rho_w}\right) g D_p}$, further introducing a shape factor $\beta_p = (A_{\text{proj},L} D_p) / \mathcal{V}_p$, as well as a modified plastic-based Eötvös (or Bond) number Γ , representing a combination of weight, buoyancy, and surface tension forces

$$\Gamma = \frac{F_B - F_W + F_\sigma}{|F_{B,\text{max}} - F_W|} = \frac{\rho_w g \mathcal{V}_{p,w} - \rho_p g \mathcal{V}_p + L_\sigma \sigma \sin(\Omega)}{g \mathcal{V}_p (|\rho_w - \rho_p|)}, \quad (12)$$

where absolute values $|\rho_w - \rho_p|$ are introduced to account for positively and negatively buoyant plastic particles, and $F_{B,\text{max}}$ stands for the maximum buoyancy force. Rearrangement yields a concise expression for the dimensionless particle velocity Θ_p

$$\Theta_p = \frac{u_p}{\sqrt{\left(\frac{|\rho_w - \rho_p|}{\rho_w}\right) g D_p}} = \frac{\ln\left(\frac{H}{z_0}\right)}{0.467 \kappa} \frac{\sqrt{\frac{2\Gamma}{\beta_p C_{L,t}}}}{1 + \sqrt{\frac{\rho_a A_{\text{proj},a}}{\rho_w A_{\text{proj},w}}}}. \quad (13)$$

2.2 Detachment velocity

In this section, the position of a plastic particle as it is detaching from the interface is considered, allowing us to develop dimensional and dimensionless formulations for the surface detachment velocity, which can be regarded as the counterpart to well-known threshold velocity formulations for bed entrainment (Dey, 2014, Chapter 4.3). Herein, surface detachment formulations are presented for both, an arbitrarily shaped particle and a cubical particle, while spherical particles are discussed in more detail in § Appendix A. Note that detachment conditions are indicated with the subscript “cr”, and they apply to the parameters u_p , $\mathcal{V}_{p,w}$, L_σ , and $A_{\text{proj},a}/A_{\text{proj},w}$. Inserting these conditions into Eq. (11) yields a general formulation for the critical particle velocity $u_{\text{cr},p}$ at surface detachment

$$u_{\text{cr},p} = \frac{\ln\left(\frac{H}{z_0}\right)}{0.467 \kappa} \frac{\sqrt{\frac{\rho_w g (\mathcal{V}_{p,w})_{\text{cr}} - \rho_p g \mathcal{V}_p + L_{\text{cr},\sigma} \sigma \sin(\Omega)}{\frac{1}{2} \rho_w C_{L,t} A_{\text{proj},L}}}}{1 + \sqrt{\frac{\rho_a}{\rho_w} \left(\frac{A_{\text{proj},a}}{A_{\text{proj},w}}\right)_{\text{cr}}}}. \quad (14)$$

which holds for all close-shaped particles. It is emphasized that Eq. (14) resembles a novel formulation for the detachment of floating plastics from the free-surface of an open-channel flow, where the critical velocity $u_{\text{cr},p}$ decreases with increasing bed roughness, particle weight, and hydrodynamic lift, while it increases with increasing water depth, surface tension, and buoyancy.

Next, let us define the detachment condition for a floating cubical particle. In view of Fig. 1b, it becomes clear that detachment happens as the cubical particle is almost fully submerged, but still exposed to surface tension forces. In order to express this condition mathematically, the relative submergence of the particle is defined as h_w/a , where a is the side length, and h_w is the submerged depth (Fig. 1b). At detachment, the relative submergence $(h_w/a)_{\text{cr}} \approx 1$, which implies that $(A_{\text{proj},a}/A_{\text{proj},w})_{\text{cr}} \approx 0$. Inserting these conditions into Eq. (14), one can simplify

$$(u_{\text{cr},p})_{\text{cube}} = \frac{\ln\left(\frac{H}{z_0}\right)}{0.467 \kappa} \sqrt{\frac{ga^2(\rho_w - \rho_p) + 4\sigma \sin(\Omega)}{\frac{1}{2} \rho_w C_{L,t} a}}, \quad (15)$$

where $\mathcal{V}_p = a^3$, $(\mathcal{V}_{p,w})_{\text{cr}} = a^3$, $L_{\text{cr},\sigma} = 4a$, and $A_{\text{proj},L} = a^2$ have been used.

In a next step, a generalized dimensionless version of the critical detachment velocity is obtained by inserting the detachment conditions for the parameters Θ_p , u_p , Γ , and $A_{\text{proj},a}/A_{\text{proj},w}$ into Eq. (13), yielding

$$\Theta_{\text{cr},p} = \frac{u_{\text{cr},p}}{\sqrt{\left(\frac{|\rho_w - \rho_p|}{\rho_w}\right) g D_p}} = \frac{\ln\left(\frac{H}{z_0}\right)}{0.467 \kappa} \frac{\sqrt{\frac{2\Gamma_{\text{cr}}}{\beta_p C_{L,t}}}}{1 + \sqrt{\frac{\rho_a}{\rho_w} \left(\frac{A_{\text{proj},a}}{A_{\text{proj},w}}\right)_{\text{cr}}}}, \quad (16)$$

which can be regarded as the surface detachment counterpart of the well-known Shields parameter for bed entrainment. Importantly, detachment conditions need to be defined for each particle shape. For a cubical particle, Eq. (16) simplifies to

$$(\Theta_{\text{cr},p})_{\text{cube}} = \frac{u_{\text{cr},p}}{\sqrt{\left(\frac{|\rho_w - \rho_p|}{\rho_w}\right) g D_p}} = \frac{\ln\left(\frac{H}{z_0}\right)}{0.467 \kappa} \sqrt{\frac{2\Gamma_{\text{cr}}}{C_{L,t} \beta_p}}, \quad (17)$$

where $\Gamma_{\text{cr}} = (\rho_w - \rho_p)/(|\rho_w - \rho_p|) + 4\sigma \sin(\Omega)/ga^2(|\rho_w - \rho_p|)$, as per Eq. (12).

To provide a preliminary assessment of the derived formulations, Eq. (15) is evaluated for a cubical particle floating at the free-surface of an open channel flow, the latter characterised by a ratio of water depth to hydraulic roughness $H/z_0 = 100$. To account for surface tension, an interfacial contact length $L_\sigma = 4a$, surface tension of $\sigma =$

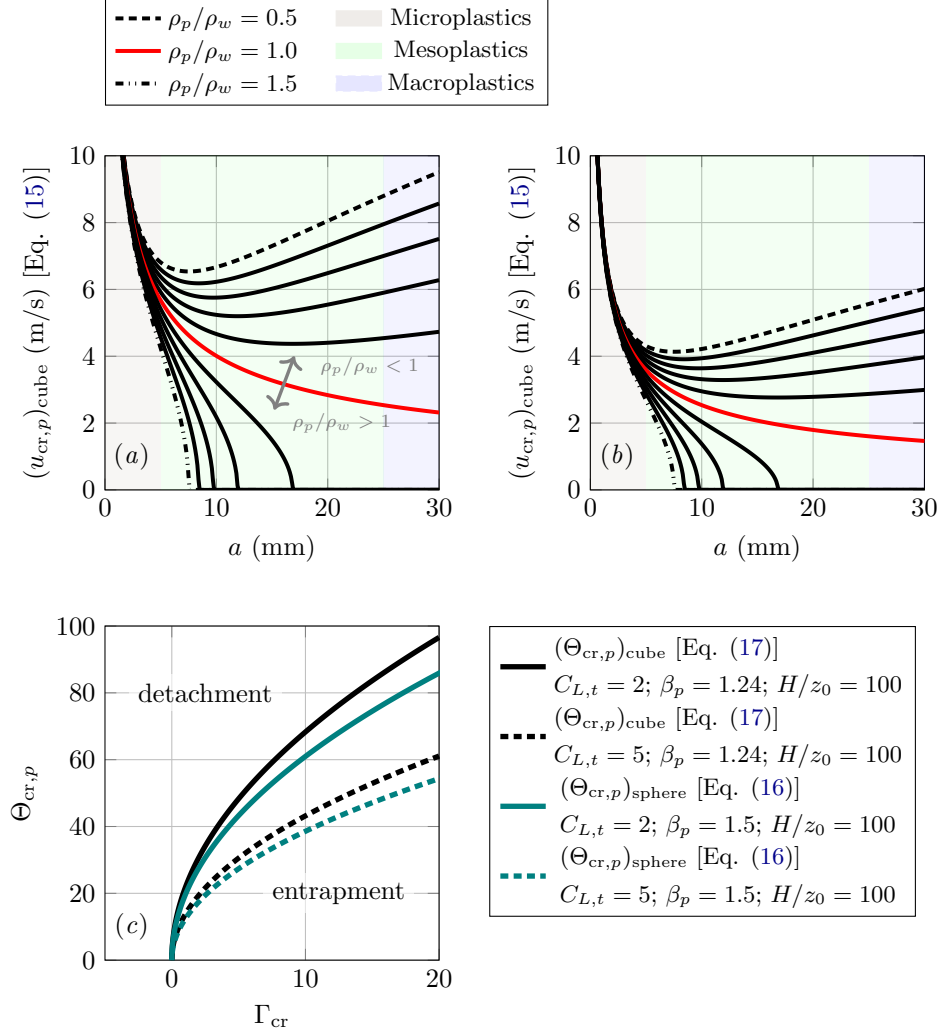


Figure 2. Critical particle detachment velocity: (a) dimensional detachment velocity for a cubical plastic versus particle size for a turbulent lift coefficient $C_{L,t} = 2$; the simulated channel is characterised by $H/z_0 = 100$; (b) same as (a) but with $C_{L,t} = 5$; (c) dimensionless critical detachment velocity Θ_{cr} versus inverse plastic-based Eötvös number Γ_{cr} at detachment; note that the shape factors $\beta_p = 1.24$ and 1.5 reflect a cubical and a spherical particle, respectively

0.072 N/m, and an interfacial contact angle $\Omega = 105^\circ$ are assumed, which is aligned with previously measured contact angles for plastics, for example $97.0^\circ \pm 0.8^\circ$ (Vlaeva et al., 2012, PP at 25° C), $96.5^\circ \pm 3.4^\circ$ (de Luna et al., 2014, HDPE at 25° C), between 93° and 105° (Diversified Enterprises, 2009a, PE), and between 95° and 117° (Diversified Enterprises, 2009b, PP). Taking the above into consideration, Eq. (15) is solved for particle dimensions between $0 \leq a \leq 30$ mm, thereby accounting for micro- ($a < 5$ mm), meso- ($5 \leq a \leq 25$ mm), and macroplastics ($a > 25$ mm). Note that in the absence of better knowledge, turbulent lift coefficients of $C_{L,t} = 2$ and 5 have been selected, which requires experimental verification. Figures 2a,b show the results of this analysis, where $u_{cr,p}$ is plotted against a for eleven different density ratios, ranging from $0.5 \leq \rho_p/\rho_w \leq 1.5$, separated by increments of 0.1 . Neutrally buoyant particles are indicated by the red

lines, whereas positively and negatively buoyant particles are located above and below these solutions, respectively. In terms of physical implications for plastic surface load transport, it becomes clear that the free-surface acts as sink for microplastics, regardless of their density, which is further corroborated by the equivalent results for spherical particles (§ Appendix A). In contrast, negatively buoyant meso- and macroplastics, which are transported to the free-surface by turbulent diffusion, are most likely detaching from this interface.

The evaluation of the dimensionless Eq. (17) for cubical particles is straightforward, and $(\Theta_{cr,p})_{\text{cube}}$ is herein computed using $H/z_0 = 100$, $\kappa = 0.41$, $(\beta_p)_{\text{cube}} = \sqrt[3]{6/\pi} = 1.24$, further assuming two lift coefficients, $C_{L,t} = 2$ and 5. Figure 2c shows these results, where dimensionless particle velocities $\Theta_p < \Theta_{cr,p}$ and $\Theta_p \geq \Theta_{cr,p}$ indicate surface entrapment and detachment, respectively. For spherical particles, the term $(A_{\text{proj},a}/A_{\text{proj},w})_{\text{cr}} > 0$, which requires an evaluation of Eq. (16). Such calculations are a bit more involved and are presented in more detail in § Appendix A, while the results have been added to Fig. 2c, demonstrating detachment velocities for spherical particles are smaller than for cubical particles, which is because $(L_{cr,\sigma})_{\text{sphere}} < (L_{cr,\sigma})_{\text{cube}}$, given that $(D_p)_{\text{sphere}} = (D_p)_{\text{cube}}$. Overall, most of the parameters in the generalized equations for surface detachment, i.e., Eqns. (14) and (16), can be determined or estimated, however, the surface tension force and the turbulent lift coefficient $C_{L,t}$ require future detailed experimental investigations, which are however beyond the scope of the present work. Lastly, it is stressed that Fig. 2c reflects the surface detachment counterpart of the Shields diagram for bed entrainment, and that the novel formulations, i.e., Eqns. (14) or (16), can be implemented into Lagrangian particle tracking simulations with relative ease.

3 Bed entrainment

3.1 Plastic Shields parameter

To derive an expression for the plastic Shields parameter, let us consider a plastic particle to be located on a sediment bed (Fig. 3), where the latter is characterised by its characteristic diameter d_{50} . The particle is subject to drag force F_D , resistance force F_R , weight force F_W , buoyancy F_B , and lift F_L . It is acknowledged that consideration of these forces corresponds to many derivations that exist for natural sediments, and the reader is referred to Dey (2014, Chapter 4) for an overview. As the flowrate increases gradually, the plastic particle will eventually start moving. The corresponding velocity at particle level, which is adequate to initiate particle motion, is commonly referred to as critical velocity u_{cr} . In contrast to the critical particle velocity at the free-surface, introduced in § 2, the critical velocity u_{cr} refers to the streamwise velocity of the fluid in vicinity of the channel bed.

The application of Newton's second law to the plastic particle in horizontal direction yields (Fig. 3)

$$\underbrace{\frac{1}{2}\rho_w u_{cr}^2 C_{D,p} A_{\text{proj}}}_{=F_D} = \underbrace{\left((\rho_p - \rho_w)gV_p - \frac{1}{2}\rho_w u_{cr}^2 C_{L,p} A_{\text{proj}} \right) \tan(\phi_p)}_{=F_R}, \quad (18)$$

where $C_{D,p}$ and $C_{L,p}$ are the plastic drag and lift coefficients, A_{proj} is the projected area, $\tan(\phi_p)$ expresses the friction coefficient between the plastic and underlying sediment bed, and it is implied that the rate of change of particle momentum is zero. The hydrodynamic force on the sediment particle in Fig. 3 is composed of hydrodynamic drag and hydrodynamic lift, which are dependent on the particle Reynolds number $Re_p = (u_{cr}D_p)/\nu$. We note that the plastic particle is subject to a velocity gradient, and a strong dependence of drag and lift with respect to the shear rate can be expected. Further, the lift force at entrainment may comprise several components, including shear lift, Magnus lift,

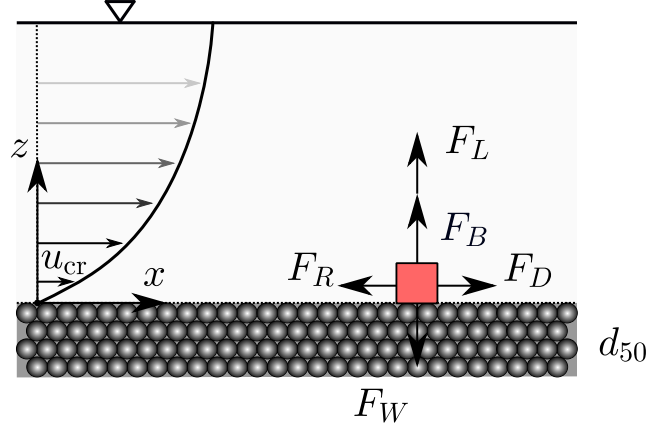


Figure 3. Forces acting on a deposited plastic particle in an open-channel flow; the sediment bed is characterised by its median grain size d_{50}

centrifugal lift, and turbulent lift, while it is stressed that there is no generic consensus on the lift force at particle entrainment (Dey et al., 2020). Nonetheless, the lift force is kept in the following, as it is regarded important for incipient motion.

Rearranging and simplifying Eq. (18) as per § Appendix B leads to a definition of the plastics Shields parameter $\theta_{cr,p}$

$$\theta_{cr,p} = \frac{\tau_{cr,p}}{(\rho_p - \rho_w)gD_p} = \frac{2}{\beta_p} \underbrace{\frac{1}{\alpha_p^2}}_{=f(Re_*, \frac{D_p}{d_{50}})} \underbrace{\frac{\tan(\phi_p)}{C_{D,p} + C_{L,p} \tan(\phi_p)}}_{=f(Re_*, \alpha_p, \frac{D_p}{d_{50}})}, \quad (19)$$

where $\tau_{cr,p}$ is the critical shear stress at entrainment, the parameter $\alpha_p = u_{cr}/u_*$ accounts for deviations between the critical velocity u_{cr} and the shear velocity $u_* = \sqrt{\tau_{cr,p}/\rho_w}$, and the parameter $\beta_p = (A_{proj}D_p)/V_p$ is a shape factor. We note that the term $1/\alpha_p^2$ is a function of D_p/d_{50} and of the shear Reynolds number $Re_* = (u_*d_{50})/\nu$, whereas the combined drag-lift-friction term on the right hand side of Eq. (19) is a function of D_p/d_{50} and of the particle Reynolds number Re_p . Importantly, particle and shear Reynolds numbers are related to one another by

$$\frac{Re_p}{Re_*} = \frac{u_{cr} D_p}{u_* d_{50}} = \alpha_p \frac{D_p}{d_{50}}, \quad (20)$$

which allows us to write Eq. (19) as function of Re_* , α_p , and D_p/d_{50} only. At this stage, it is important to recall that the incipient motion of plastic particles on a sediment layer is *fully explained* by Eq. (19). The unknowns are the parameters α_p and β_p , the friction angle ϕ_p , as well as plastic drag and lift coefficients, $C_{D,p}$ and $C_{L,p}$.

Figure 4 shows the classical Shields diagram, where the Shields parameter is plotted against the shear Reynolds number. Here, microplastic data (Waldschläger & Schüttrumpf, 2019b; Goral et al., 2023) have been included, and, for comparison, an analytical expression for the critical Shields parameter of natural sediments $\theta_{cr,s}$ (Sui et al., 2021)

$$\theta_{cr,s} = 0.165(Re_* + 0.6)^{-0.8} + 0.045 \exp(-40 Re_*^{-1.3}). \quad (21)$$

It is seen that plastics have a higher mobility when compared to natural sediment (Fig. 4), and that there is a large variability in the collected plastic data, which stems

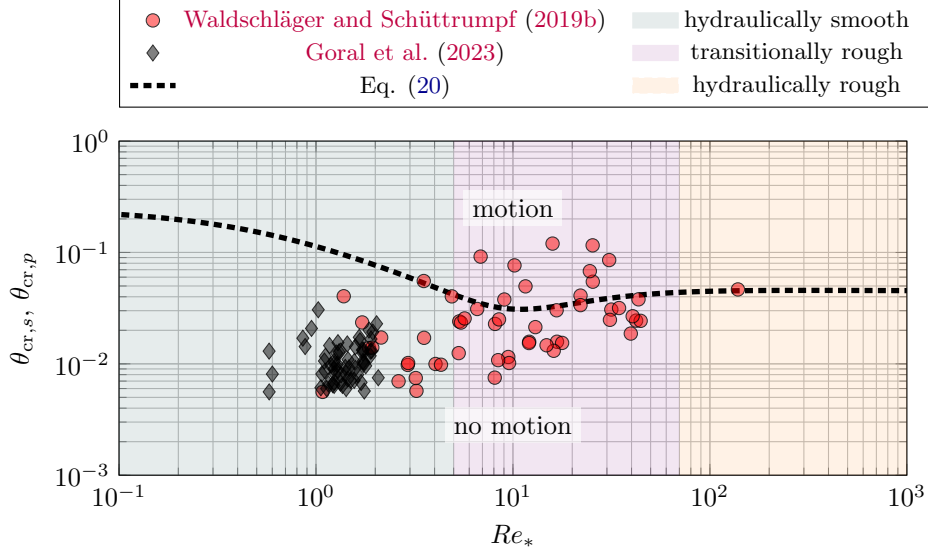


Figure 4. Classical Shield diagram for sediment particles; plastic data are computed and plotted for the experiments of [Waldschläger and Schüttrumpf \(2019b\)](#) and [Goral et al. \(2023\)](#); the flow regimes are classified as hydraulically smooth flow for $Re_* \leq 5$, as hydraulically transitional flow for $5 < Re_* < 70$, and as hydraulically rough flow for $Re_* \geq 70$

from different shapes and materials, but also from different sizes of the tested particles. If one was to establish a Shields curve for plastics as a complement to Eq. (21), some comprehensive testing, encompassing a wide range of plastic shapes, materials, and sizes would be required. It is also anticipated that there is not one general Shields curve for plastics, but rather different curves for different plastic shapes.

3.2 Plastic-sediment interrelation

To advance knowledge on the incipient motion of plastic particles, it seems intuitive to seek a relationship between the plastic Shields parameter $\theta_{cr,p}$ and the well-known Shields parameter for natural sediment $\theta_{cr,s}$, which is presented in the following. Similar to the derivation of Eq. (19), linear momentum conservation is applied to a sediment particle on a sediment bed, leading to an analytical equation for the sediment Shields parameter ([Wiberg & Smith, 1987](#); [Dey, 2014](#))

$$\theta_{cr,s} = \frac{\tau_{cr,s}}{(\rho_s - \rho_w) g D_s} = \frac{2}{\beta_s} \underbrace{\frac{1}{\alpha_s^2}}_{=f(Re_*)} \underbrace{\frac{\tan(\phi_s)}{C_{D,s} + C_{L,s} \tan(\phi_s)}}_{=f(Re_*, \alpha_s)}, \quad (22)$$

where the subscript s stands for sediment. We note that for natural sediments, $D_s \approx d_{50}$, which implies that the dependence on D_s/d_{50} vanishes, i.e., $Re_s = \alpha_s Re_*$. Dividing Eq. (19) by Eq. (22) yields two expressions that relate the plastic Shields parameter to the sediment Shields parameter

$$\frac{\theta_{cr,p}}{\theta_{cr,s}} = \frac{\tau_{cr,p}}{\tau_{cr,s}} \frac{(\rho_s - \rho_w)}{(\rho_p - \rho_w)} \frac{D_s}{D_p} \quad (23)$$

$$= \frac{\beta_s}{\beta_p} \frac{\alpha_s^2}{\alpha_p^2} \frac{C_{D,s} + C_{L,s} \tan(\phi_s)}{C_{D,p} + C_{L,p} \tan(\phi_p)} \frac{\tan(\phi_p)}{\tan(\phi_s)}. \quad (24)$$

It is important to note that Eqns. (23) and (24) are not only applicable to plastics. Rather, they can be used to relate any Shields parameter of a foreign particle p to the Shields parameter of natural sediment, thereby representing a general and versatile framework. Note that there exists a variety of other expressions for the Shields parameter, some of them summarised in [Dey \(2014, Chapter 4\)](#), which could alternatively be used to derive a relationship between the onset of motion of plastics and sediments.

In the context of practical application of the proposed framework, it is important to give considerations to the flow situations that are being related to one another. For example, one might be interested in comparing the incipient motion of foreign particles with sediment particles assuming identical Re_* , which could further imply $D_s = d_{50}$, while the diameter of the foreign particle could be smaller or larger than the sediment particle, i.e., $D_p < D_s$ or $D_p > D_s$. To provide a second example, if the foreign particle is natural sediment with $D_p = D_s = d_{50}$, $\rho_p = \rho_s$, and other parameters being identical, the right hand sides of Eqns. (23) and (24) become unity, implying that the classical Shields diagram is recovered, i.e., $\theta_{cr,p} = \theta_{cr,s}$. Further, some of the involved terms, for example drag and lift coefficients of partially exposed plastics and sediments in the bed-boundary layer, are not well understood, which is one of the main reasons that the sediment Shields curve is of semi-empirical nature. Therefore, simplifications are required to proceed. Adopting the approach from [Wilcock \(1988, Eq. 12\)](#), one can postulate that

$$\frac{\tau_{cr,p}}{\tau_{cr,s}} = \left(\frac{D_p}{D_s} \right)^{c_3}, \quad (25)$$

which can be combined with Eq. (23) to yield

$$\frac{\theta_{cr,p}}{\theta_{cr,s}} = \frac{(\rho_s - \rho_w)}{(\rho_p - \rho_w)} \left(\frac{D_p}{D_s} \right)^{c_3 - 1}, \quad (26)$$

where c_3 is an unknown exponent. Upon comparing Eq. (26) with the empirical Eq. (1), it is realized that $c_2 = c_3 - 1$ and that $c_1 = (\rho_s - \rho_w)/(\rho_p - \rho_w)$, where the latter may range between $5.5 < c_1 < 16.5$, which was estimated using $\rho_s = 2650 \text{ kg/m}^3$, $\rho_w = 1000$, and $\rho_p = 1100$ to 1300 kg/m^3 . As such, there are large discrepancies between the empirically determined $c_1 = 0.5588$ ([Waldschläger & Schüttrumpf, 2019b](#)) and estimated parameter values $5.5 < c_1 < 16.5$, which leads to the conclusion that [Wilcock's \(1988\)](#) approach of expressing critical shear stresses through a hiding-exposure function, i.e., Eq. (25), may not be applicable to plastics; it is important to note that the general concept of a hiding-exposure function remains physically meaningful, as shown in the following.

Moving on to Eq. (24), this expression can be reconciled with previously suggested empirical approaches ([Waldschläger & Schüttrumpf, 2019b](#); [Goral et al., 2023](#)) by making some crude assumptions, namely

$$\frac{\theta_{cr,p}}{\theta_{cr,s}} = \frac{\beta_s \tan(\phi_p)}{\beta_p \tan(\phi_s)} \underbrace{\frac{\alpha_s^2 C_{D,s} + C_{L,s} \tan(\phi_s)}{\alpha_p^2 C_{D,p} + C_{L,p} \tan(\phi_p)}}_{\left(\frac{D_p}{D_s} \right)^{c_2}}, \quad (27)$$

which leads to a rather simplistic expression of the Shields parameter ratio

$$\frac{\theta_{cr,p}}{\theta_{cr,s}} = \frac{\beta_s \tan(\phi_p)}{\beta_p \tan(\phi_s)} \left(\frac{D_p}{D_s} \right)^{c_2}. \quad (28)$$

We note that Eq. (28) constitutes an expansion of the approach suggested by [Waldschläger and Schüttrumpf \(2019a, Eq. 4\)](#) and [Goral et al. \(2023, Eq. 16\)](#), based on a rigorous application of linear momentum conservation. Importantly, this expanded approach explicitly takes into account the particle shape by retaining the term β_s/β_p . The derivation

also demonstrates that different physical effects have been lumped into a single hiding-exposure function, and these simplifications need to be carefully examined. Depending on the particle shape, one may argue that $\alpha_s^2/\alpha_p^2 \propto (D_p/D_s)^{c_4}$, with c_4 being an unknown exponent. However, other terms, such as the particle drag and lift coefficients are dependent on the particle Reynolds numbers, and these Reynolds-number effects may not be accounted for. As outlined before, there is an imminent need for more fundamental testing on the mobilization of plastics, which should scrutinize how Eq. (24), or other versions thereof, can be simplified.

3.3 Data re-analysis

In this section, the expanded approach for estimating plastic Shields parameters [Eq. (28)] is applied to previous experimental data sets from literature. Note that the incipient motion of plastics and sediments is compared for identical Re_* , which is the most natural choice, as the calculation of particle Reynolds numbers would require some assumptions in the determination of α_p and α_s . In a first step of the conducted re-analysis, published data from [Waldschläger and Schüttrumpf \(2019b\)](#) and [Goral et al. \(2023\)](#) are used to calculate plastic Shields parameters as $\theta_{cr,p} = u_* / ((\rho_p/\rho_w - 1)gD_p)$ [Eq. (B4)]. Subsequently, Eq. (21) is applied to estimate corresponding sediment Shields parameters, where the shear Reynolds number is calculated as $Re_* = (u_*d_{50})/\nu$. Following [Goral et al. \(2023\)](#), friction terms for both experiments are assumed as $\tan \theta_p / \tan \theta_s = 0.5588$ and 0.55, respectively. Subsequently, the sediment shape factor is considered as $\beta_s = 1.5$ (spherical), while plastic shape factors β_p are computed using geometric particle specifications provided in Tab. 1. It is noted that the determination of β_p for some tested shapes, such as fragments, fibers, etc., is not straightforward, and for those shapes, it is simply assumed $\beta_p/\beta_s = 1$, which allows to retain these data.

Table 1. Shape factors $\beta_p = (A_{proj}D_p)/\mathcal{V}_p$ for selected plastic geometries; note that the diameters are calculated as sphere-volume equivalent diameter $D_p = \sqrt[3]{\frac{6}{\pi}\mathcal{V}_p}$

Shape/ Parameter	Sphere	Cylinder	Cube	Rectangular prism
\mathcal{V}_p (m ³)	$\frac{\pi D_p^3}{6}$	$\frac{\pi D^2 a}{4}$	a^3	abc
A_{proj} (m ²)	$\frac{\pi D_p^2}{4}$	aD	a^2	bc
D_p (m)	D_p	$\sqrt[3]{1.5D^2a}$	$\sqrt[3]{\frac{6}{\pi}}a$	$\sqrt[3]{\frac{6}{\pi}}abc$
β_p (-)	1.5	$4\sqrt[3]{1.5a}/(\pi D^{1/3})$	1.24	$\sqrt[3]{\frac{6}{\pi}}abc/a$

Next, the functional dependence between $\frac{\theta_{cr,p}}{\theta_{cr,s}} \frac{\beta_p \tan(\phi_s)}{\beta_s \tan(\phi_p)}$ and the diameter ratio D_p/D_s is evaluated, allowing to estimate the exponent c_2 of the hiding-exposure function (Fig. 5a). Minimising the root-mean-square deviation between measurements and the hiding-exposure function, it is determined that all experimental data are well represented if the exponent is set to $c_2 = -0.6$. To reconcile the incipient motion of plastics with clas-

sical sediment the plastic Shields parameter can be normalised as

$$\frac{\theta_{cr,p}}{\left(\frac{\beta_s \tan(\phi_p)}{\beta_p \tan(\phi_s)}\right) \left(\frac{D_p}{D_s}\right)^{c_2}} = \theta_{cr,s}. \quad (29)$$

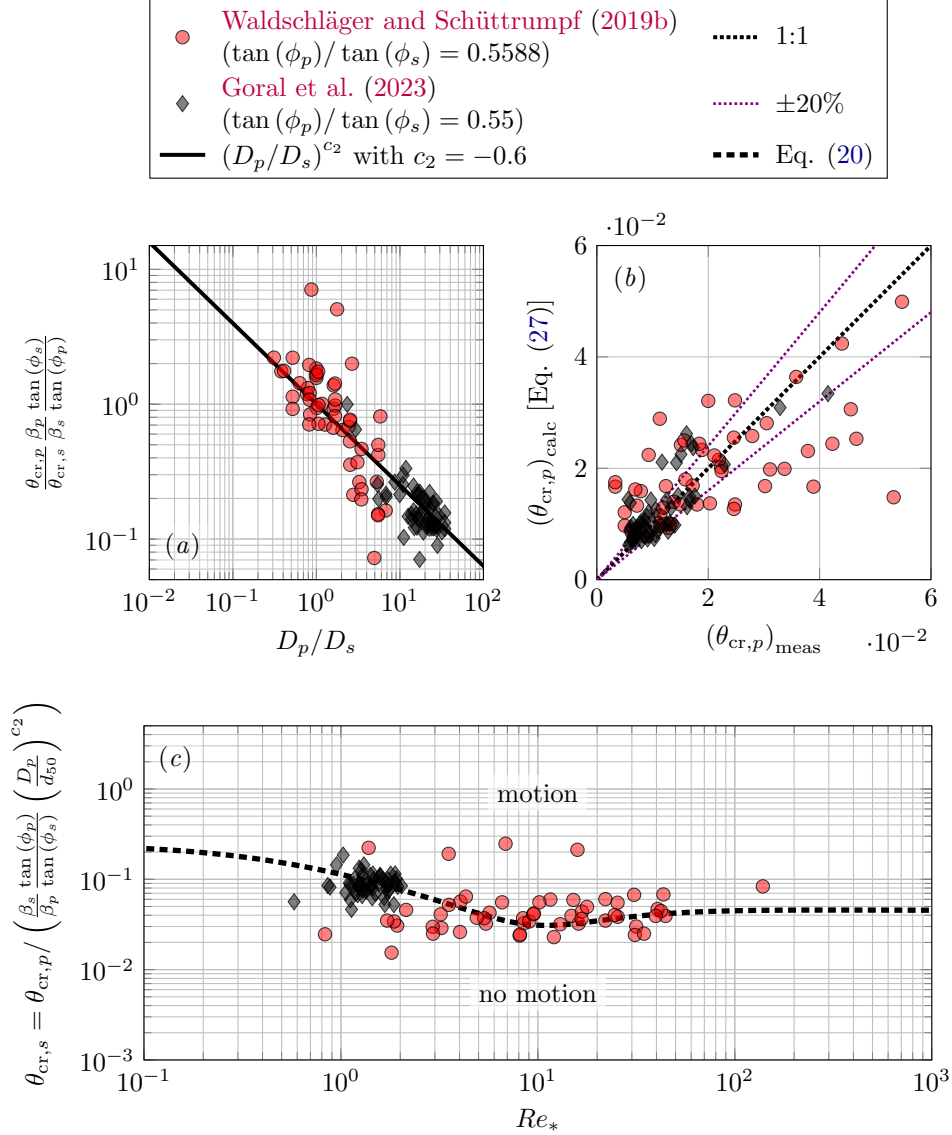


Figure 5. Incipient motion of plastic particles: (a) hiding exposure-function; (b) measured versus calculated plastic Shields parameters (c) classical Shields diagram with modified plastic Shields parameter

These normalised values are plotted together with the sediment Shields curve [Eq. (21)] in Fig. 5c. Comparing the Shields parameters of plastics with those of natural sediment (Figs. 3 and 5c), one can draw the following conclusions on how different physical parameters affect the mobility of plastics: i) the plastic shape can lead to a reduced or increased mobility of plastics compared to sediments ($\beta_s/\beta_p > 1$ or $\beta_s/\beta_p < 1$), ii)

the friction term increases the mobility of plastics ($\tan(\phi_s)/\tan(\phi_p) < 1$), and iii) the plastic size can lead to an increase in mobility if $D_p > D_s$ (exposure effect), or to a decrease if $D_p < D_s$ (hiding effect). For completeness, a plot of measured versus calculated plastic Shields parameters is shown in Fig. 5b. It is seen that there is some data scatter, which is anticipated to be caused by experimental uncertainties and by unaccounted effects deriving from simplifications made to obtain Eq. (28). Given that the tested plastic data comprise a variety of different shapes and that the classical Shields diagram for sediments holds a similar level of scatter, the present approach seems reasonable, and it is believed that the proposed framework provides a valuable basis for future research on this topic.

4 Conclusion

This work is inspired by the fact that many numerical studies of fluvial plastic transport are treating their particles as “settled” or “surfaced” once they reach the bottom boundary or the free-surface in their simulations, revealing an imminent knowledge gap in the understanding of free-surface detachment and bed entrainment of plastic particles. To close this gap, a first principle approach is deployed, enabling the derivation of a novel formulation for free-surface detachment of floating plastics, as well as the creation of a surface detachment/entrainment diagram, which can be regarded as the surface counterpart to the classical Shields diagram. It is acknowledged that some of the parameters relating to surface tension and turbulent lift must be validated or established in physical experiments. A preliminary analysis of the critical detachment velocity, exemplified for cubical and spherical particles, shows that the free-surface acts as sink for microplastics, while larger plastics are likely to detach from the interface. We anticipate that the implementation of this formulation into numerical modelling environments will allow for a more realistic prediction of plastic surface transport processes.

Next, the focus is set on bed entrainment (or incipient motion) of fluvial plastics, and a formulation of the plastic Shields parameter is presented, which is in principle identical to formulations used for natural sediment. Because the establishment of a plastic Shields curve would require dozens of experiments, a time-saving alternative is desired. This is herein achieved by introducing a framework that relates different Shields parameters with one another, thereby allowing to reconcile incipient motion conditions of plastics with those of natural sediments. It is noted that this framework i) is based on first principles, ii) leads to a new expression for the plastic Shields parameter, which represents an expansion of previous approaches used in plastic research, and iii) explicitly accounts for the particle shape. Subsequently, this new framework is tested using two data sets from literature, and a reasonable agreement between predictions and measurements is achieved, while some assumptions need to be scrutinised in the future. Altogether, it is hoped that this work on surface detachment and bed entrainment will be useful for the planning, execution, and analysis of future experiments and simulations of turbulent plastic transport in an environmental fluid mechanics context.

Open Research Section

Supporting data used to create figures in this manuscript is associated with the studies from [Waldschläger and Schüttrumpf \(2019b\)](#) and [Goral et al. \(2023\)](#). These data can be downloaded from [Link 1](#) and [Link 2](#).

Acknowledgments

I would like to thank Deniz Goral and David R. Fuhmann for fruitful discussions on bed entrainment of plastics. Further, I acknowledge the exchanges with my PhD students Felipe Condo and Charuni Wickramarachchi, as well as with my colleague Daniel Valero.

Notation

The following symbols and abbreviations are used in this manuscript:

Parameters

$a, b,$ and c	geometrical dimensions as per Tab. 1 (m)
A_{proj}	projected area for drag and lift (m^2)
$A_{\text{proj},L}$	projected area for turbulent lift (m^2)
c_1 to c_4	empirical parameters for hiding-exposure function (–)
C_D	drag coefficient (–)
C_L	lift coefficient (–)
$C_{L,t}$	turbulent lift coefficient (–)
D	diameter of cylinder base (m)
D_p	sphere-volume equivalent diameter (m)
R_p	radius of spherical particle (m)
d_{50}	median diameter of underlying sediment (m)
F_B	buoyancy force (N)
F_D	drag force (N)
F_L	lift force (N)
F_R	resistance force (N)
F_W	weight force (N)
F_σ	surface tension force (N)
g	gravitational acceleration (m/s^2)
h_w	submerged depth (m)
H	water depth (m)
L_σ	air-water-plastic interface length (m)
Re_p	plastic Reynolds number (–)
Re_s	sediment Reynolds number (–)
Re_*	shear Reynolds number (–)
\mathcal{V}	particle volume (m^3)
$\mathcal{V}_{p,w}$	submerged volume of plastic particle (m^3)
u_a	air velocity of the air-superlayer (m/s)
u_{fs}	fluid surface velocity (m/s)
u_p	velocity of surfaced plastic (m/s)
$u_{\text{cr},p}$	critical velocity for surface detachment (m/s)
u_{cr}	critical velocity for bed entrainment (m/s)
u_*	bed shear velocity (m/s)
v'_{rms}	root-mean-square of vertical velocity fluctuations (m/s)
x	streamwise coordinate (m)
z	vertical coordinate (m)
z_0	hydraulic roughness (m)
α	$= u_{\text{cr}}/u_*$; deviation parameter (–)
β	$= (A_{\text{proj}}D)/\mathcal{V}$; particle shape factor (–)
Γ	plastic-based Eötvös number (–)
θ_{cr}	Shields parameter (–)
$\Theta_{\text{cr},p}$	dimensionless surface detachment velocity (–)
κ	van Karman constant (–)
ν	kinematic water viscosity (m^2/s)
ρ	density (kg/m^3)
σ	surface tension (N/m)
τ_{cr}	critical bed shear stress (N/m^2)
ϕ	friction angle ($^\circ$)
Ω	contact angle ($^\circ$)

Indices and abbreviations

a	air
cube	cubical particle
cr	critical
max	maximum
p	plastic
s	sediment
sphere	spherical particle
w	water

Appendix A Detachment of spherical particles

To formulate the detachment condition for spherical particles, let us consider a floating plastic sphere shown in Fig. A1a, subject to buoyancy F_B , surface tension F_σ , weight force F_W , and turbulent lift F_L . Here, D_p and h_w are the diameter and the submerged depth, respectively. Considering the forces acting on the spherical particle, it becomes clear that the interfacial contact length L_σ is a function of h_w , and that i) $L_\sigma \rightarrow 0$ as $h_w \rightarrow D_p$, and ii) $L_\sigma \rightarrow \max$ as $h_w \rightarrow 0.5D_p$. More generally, the relative and absolute contributions of F_B , F_σ , and F_W depend on the submergence of the spherical particle, similarly discussed for plastic cups in Valero et al. (2022, Appendix B), while the projected area $A_{\text{proj,L}} = \pi R_p^2$ in Eq. (6) is perpendicular to the lift force, which suggests, in a first approximation, that F_L does not depend on h_w . As such, the detachment condition for spherical particles is postulated as

$$h_{\text{cr},w} = \arg \max_{h_w} (\rho_w g \mathcal{V}_{p,w} - \rho_p g \mathcal{V}_p + L_\sigma \sigma \sin(\Omega)), \quad (\text{A1})$$

which implies that F_L has to overcome the maximum vertical force, formed by F_B , F_σ , and F_W , for the particle to be detached. In Eq. (A1), the submerged volume of the spherical particle is $\mathcal{V}_{p,w} = \frac{\pi h_{\text{cr},w}^2}{3} (3R_p - h_{\text{cr},w})$, the total volume $\mathcal{V}_p = \frac{4}{3} \pi R_p^3$, and the interfacial contact length $L_\sigma = 2\pi \sqrt{2h_w R_p - h_w^2}$, with $R_p = D_p/2$ being the radius. Figure A1b shows the detachment condition $(h_w/D_p)_{\text{cr}}$ for spheres with diameters ranging from $D_p = 0$ to 30 mm, which was evaluated using Eq. (A1), further assuming $\sigma = 0.072$ N/m and $\Omega = 105^\circ$. Because weight and buoyant forces are negligible for small particles, $(h_w/D_p)_{\text{cr}} \approx 0.5$ for $D_p < 1$ mm, and $(h_w/D_p)_{\text{cr}}$ increases towards unity with increasing D_p . Notably, the results shown in Fig. A1b are independent of the particle density ρ_p .

Having determined $h_{\text{cr},w}$ as per Fig. A1b, detachment velocities $u_{\text{cr},p}$ for spherical particles can be evaluated using Eq. (14). Here, previously used parameter values were adopted, including $H/z_0 = 100$, $C_{L,t} = 2$ and 5, $\sigma = 0.072$ N/m, $\Omega = 105^\circ$, whereas $(\mathcal{V}_{p,w})_{\text{cr}}$, $L_{\text{cr},\sigma}$, and $\left(\frac{A_{\text{proj},a}}{A_{\text{proj},w}}\right)_{\text{cr}}$ are related to $h_{\text{cr},w}$ through

$$(\mathcal{V}_{p,w})_{\text{cr}} = \frac{\pi h_{\text{cr},w}^2}{3} (3R_p - h_{\text{cr},w}) \quad (\text{A2})$$

$$L_{\text{cr},\sigma} = 2\pi \sqrt{2h_{\text{cr},w} R_p - h_{\text{cr},w}^2}, \quad (\text{A3})$$

$$\left(\frac{A_{\text{proj},a}}{A_{\text{proj},w}}\right)_{\text{cr}} = \frac{\pi R_p^2}{R_p^2 \arccos\left(1 - \frac{h_{\text{cr},w}}{R_p}\right) \sqrt{R_p^2 - (R_p - h_{\text{cr},w})^2}} - 1. \quad (\text{A4})$$

The results of this analysis are shown in Fig. A2 for densities ranging from $0.5 \leq \rho_p/\rho_w \leq 1.5$, separated by increments of 0.1. Overall, the trends are very similar to the

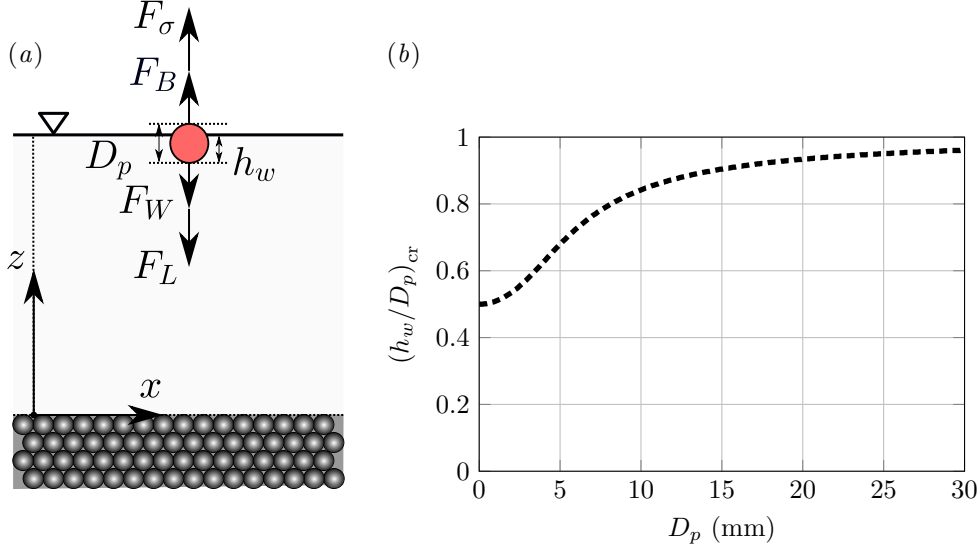


Figure A1. Detachment of spherical plastic particles: (a) conceptual sketch, including forces acting on the floating sphere; (b) relative submergence as function of the particle diameter D_p

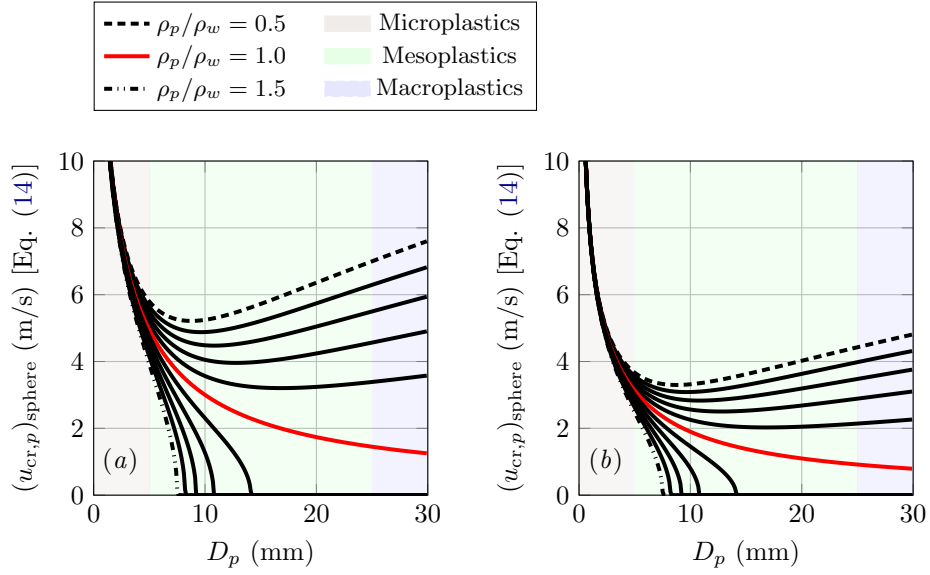


Figure A2. Critical particle detachment velocities for spherical particles: (a) dimensional detachment velocity versus particle diameter for a turbulent lift coefficient $C_{L,t} = 2$; the simulated channel is characterised by $H/z_0 = 100$; (b) same as (a) but with $C_{L,t} = 5$

detachment velocities of cubical particles, compare Fig. 2, with physical implications as discussed, while critical velocities of spherical particles are shifted to slightly smaller values when compared to cubical particles, which is due to shorter interfacial contact lengths $L_{cr,\sigma}$. Next, dimensionless detachment velocities $(\Theta_{cr,p})_{sphere}$ are calculated using Eq. (16) in combination with Eqns. (A1), (A2), (A3), and (A4), and have been shown in Fig. 2c. At last, it is noteworthy mentioning that detachment conditions for other closed-shaped

particles, such as cylinders, rectangular prisms, and ellipsoids, can easily be deduced using the detachment condition formulated in Eq. (A1).

Appendix B Plastic Shields parameter

In this section, a derivation of the plastic Shields parameter is presented, which closely follows previous works on the incipient motion of natural sediment by [Wiberg and Smith \(1987\)](#). Our starting point is the streamwise force balance on the deposited plastic at the onset of motion, i.e., Eq. (18), which is repeated for convenience

$$\frac{1}{2}\rho_w u_{\text{cr}}^2 C_{D,p} A_{\text{proj}} = \left((\rho_p - \rho_w) g \mathcal{V}_p - \frac{1}{2}\rho_w u_{\text{cr}}^2 C_{L,p} A_{\text{proj}} \right) \tan(\phi_p). \quad (\text{B1})$$

Rearranging Eq. (B1)

$$\frac{1}{2}\rho_w u_{\text{cr}}^2 A_{\text{proj}} (C_{D,p} + C_{L,p} \tan(\phi_p)) = (\rho_p - \rho_w) g \mathcal{V}_p \tan(\phi_p), \quad (\text{B2})$$

and dividing by $\frac{1}{2} A_{\text{proj}} (C_{D,p} + C_{L,p} \tan(\phi_p)) (\rho_p - \rho_w) g D_p$ yields

$$\frac{u_{\text{cr}}^2}{\left(\frac{\rho_p - \rho_w}{\rho_w} \right) g D_p} = \frac{2 \mathcal{V}_p}{A_{\text{proj}} D_p} \frac{\tan(\phi_p)}{C_{D,p} + C_{L,p} \tan(\phi_p)} \quad (\text{B3})$$

Next, a shape factor $\beta_p = (A_{\text{proj}} D_p) / \mathcal{V}_p$ and a parameter $\alpha = u_{\text{cr}} / u_*$ are introduced, where the latter accounts for deviations between the critical velocity and the shear velocity. The shear velocity is defined as $u_* = \sqrt{\tau_{\text{cr},p} / \rho_w}$, with $\tau_{\text{cr},p}$ being the critical bed shear stress. Substituting α_p and β_p into Eq. (B3) leads to the following expression of the plastic Shields parameter

$$\theta_{\text{cr},p} = \frac{u_*^2}{\left(\frac{\rho_p - \rho_w}{\rho_w} \right) g D_p} = \frac{2}{\beta_p} \frac{1}{\alpha_p^2} \frac{\tan(\phi_p)}{C_{D,p} + C_{L,p} \tan(\phi_p)}, \quad (\text{B4})$$

which can be slightly reformulated using the definition of the shear velocity

$$\theta_{\text{cr},p} = \frac{\tau_{\text{cr},p}}{(\rho_p - \rho_w) g D_p} = \frac{2}{\beta_p} \frac{1}{\alpha_p^2} \frac{\tan(\phi_p)}{C_{D,p} + C_{L,p} \tan(\phi_p)}. \quad (\text{B5})$$

References

- Bagheri, G., & Bonadonna, C. (2016). On the drag of freely falling non-spherical particles. *Powder Technology*, *301*, 526–544.
- Chubarenko, I., Bagaev, A., Zobkov, M., & Esiukova, E. (2016). On some physical and dynamical properties of microplastic particles in marine environment. *Marine Pollution Bulletin*, *108*(1), 105–112.
- Cowger, W., Gray, A. B., Guilinger, J. J., Fong, B., & Waldschläger, K. (2021). Concentration depth profiles of microplastic particles in river flow and implications for surface sampling. *Environmental Science & Technology*, *55*(9), 6032–6041.
- de Luna, M. S., Galizia, M., Wojnarowicz, J., Rosa, R., Lojkowski, W., Leonelli, C., ... Filippone, G. (2014). Dispersing hydrophilic nanoparticles in hydrophobic polymers: Hdpe/zno nanocomposites by a novel template-based approach. *eXPRESS Polymer Letters*, *8*(5), 362–372.
- Dey, S. (2014). *Fluvial hydrodynamics*. Springer.
- Dey, S., Ali, S. Z., & Padhi, E. (2020). Hydrodynamic lift on sediment particles at entrainment: present status and its prospect. *J. Hydraul. Engng.*, *146*(6). doi: 10.1061/(ASCE)HY.1943-7900.0001751

- Dey, S., Zeeshan Ali, S., & Padhi, E. (2019). Terminal fall velocity: The legacy of Stokes from the perspective of fluvial hydraulics [Journal Article]. *Proc Math Phys Eng Sci*, 475(2228), 20190277.
- Dioguardi, F., Mele, D., & Dellino, P. (2018). A new one-equation model of fluid drag for irregularly shaped particles valid over a wide range of Reynolds number. *Journal of Geophysical Research: Solid Earth*, 123(1), 144–156.
- Diversified Enterprises. (2009a). *Surface energy data for pe: Polyethylene, cas # 9002-88-4*. Retrieved from https://www.accudynetest.com/polymer_surface_data/polyethylene.pdf
- Diversified Enterprises. (2009b). *Surface energy data for pp: Polypropylene, cas #s 9003-08-0 (atactic) and 25085-53-4 (isotactic)*. Retrieved from https://www.accudynetest.com/polymer_surface_data/polypropylene.pdf
- Goral, K. D., Guler, H. G., Larsen, B. E., Carstensen, S., Christensen, E. D., Kerpen, N. B. B., ... Fuhrman, D. R. R. (2023, 2023 JUN 16). Shields diagram and the incipient motion of microplastic particles. *Environ. Sci. Technol.*. doi: 10.1021/acs.est.3c02027
- Lofty, J., Valero, D., Wilson, C., Franca, M., & Ouro, P. (2023). Microplastic and natural sediment in bed load saltation: Material does not dictate the fate. *Water Research*, 243, 120329.
- Nezu, I., & Nakagawa, H. (1993). Turbulence in open-channel flows. In *Ser., a* (pp. 1–281).
- Rohais, S., Armitage, J. J., Romero-Sarmiento, M.-F., Pierson, J.-L., Teles, V., Bauer, D., ... Pelerin, M. (2024). A source-to-sink perspective of an anthropogenic marker: A first assessment of microplastics concentration, pathways, and accumulation across the environment. *Earth-Science Reviews*, 254, 104822.
- Sui, T., Staunstrup, L. H., Carstensen, S., & Fuhrman, D. R. (2021). Span shoulder migration in three-dimensional current-induced scour beneath submerged pipelines. *Coast. Engng.*, 164. doi: 10.1016/j.coastaleng.2020.103776
- Valero, D., Belay, B. S., Moreno-Rodenas, A., Kramer, M., & Franca, M. J. (2022). The key role of surface tension in the transport and quantification of plastic pollution in rivers. *Water Research*, 226, 119078.
- Van Melkebeke, M., Janssen, C., & De Meester, S. (2020). Characteristics and sinking behavior of typical microplastics including the potential effect of biofouling: Implications for remediation [Journal Article]. *Environ Sci Technol*, 54(14), 8668-8680.
- Vlaeva, I., Yovcheva, T., Viraneva, A., Kitova, S., Exner, G., Guzhova, A., & Galikhanov, M. (2012). Contact angle analysis of corona treated polypropylene films. *Journal of Physics: Conference Series*, 398(012054).
- Waldschläger, K., Brückner, M. Z., Carney Almroth, B., Hackney, C. R., Adyel, T. M., Alimi, O. S., ... Wu, N. (2022). Learning from natural sediments to tackle microplastics challenges: A multidisciplinary perspective. *Earth-Science Reviews*, 228, 104021.
- Waldschläger, K., & Schüttrumpf, H. (2019a). Effects of particle properties on the settling and rise velocities of microplastics in freshwater under laboratory conditions. *Environmental Science & Technology*, 53(4), 1958-1966.
- Waldschläger, K., & Schüttrumpf, H. (2019b). Erosion behavior of different microplastic particles in comparison to natural sediments. *Environ. Sci. Technol.*, 53(22), 13219-13227. doi: 10.1021/acs.est.9b05394
- White, F. M. (2016). *Fluid mechanics, 8th edition* [Book]. McGraw Hill.
- Wiberg, P. L., & Smith, J. D. (1987). Calculations of the critical shear stress for motion of uniform and heterogeneous sediments. *Water Resources Research*, 23(8), 1471-1480. doi: <https://doi.org/10.1029/WR023i008p01471>
- Wilcock, P. R. (1988). Methods for estimating the critical shear-stress of individual fractions in mixed-size sediment. *Water Resour. Res.*, 24(7), 1127-1135.

- Yu, Z., Loewen, M., Guo, S., Guo, Z., & Zhang, W. (2023). Investigation of the sheltering effects on the mobilization of microplastics in open-channel flow. *Environmental Science & Technology*, *57*(30), 11259-11266.
- Yu, Z., Yao, W., Loewen, M., Li, X., & Zhang, W. (2022). Incipient motion of exposed microplastics in an open-channel flow. *Environmental Science & Technology*, *56*(20), 14498-14506.